

GEOMETRIC POTENTIAL OF CARTOSAT-1 STEREO IMAGERY

M. Crespi^{*°}, F. Fratarcangeli^{*}, F. Giannone^{*}, G. Colosimo^{*}, F. Pieralice^{*}, K. Jacobsen^{**°°}

^{*} DITS – Area di Geodesia e Geomatica – Sapienza Università di Roma– via Eudossiana 18 – Rome, Italy -
<attia.crespi,francesca.fratarcangeli,francesca.giannone>@uniroma1.it

^{**}Institute of Photogrammetry and Geoinformation
Leibniz University Hannover
jacobsen@ipi.uni-hannover.de

[°] Principal Investigator for ISPRS-ISRO C-SAP TS-6 and additional TS-Castelgandolfo

^{°°} Co-Investigator for ISPRS-ISRO C-SAP TS-5 and TS-9

SS 11, CARTOSAT-SAP

KEY WORDS: Photogrammetry, Digital, Geometry, Calibration, Block, Accuracy

ABSTRACT:

Cartosat-1 satellite, launched by Department of Space (DOS), Government of India, is dedicated to stereo viewing for large scale mapping and terrain modelling applications. This stereo capability fills the limited capacity of very high resolution satellites for three-dimensional point determination and enables the generation of detailed digital elevation models (DEMs) not having gaps in mountainous regions like for example the SRTM height model.

The Cartosat-1 sensor offers a resolution of 2.5m GSD in panchromatic mode. One CCD-line sensor camera is looking with a nadir angle of 26° in forward direction, the other 5° aft along the track.

The Institute “Area di Geodesia e Geomatica” - Sapienza Università di Roma and the Institute of Photogrammetry and Geoinformation, Leibniz University Hannover participated at the ISPRS-ISRO Cartosat-1 Scientific Assessment Programme (C-SAP), in order to investigate the generation of Digital Surface Models (DSMs) from Cartosat-1 stereo scenes.

The aim of this work concerns the orientation of Cartosat-1 stereo pairs, using the given RPCs improved by control points and the definition of an innovative model based on geometric reconstruction, that is used also for the RPC extraction utilizing a terrain independent approach. These models are implemented in the scientific software (SISAR- Software per Immagini Satellitari ad Alta Risoluzione) developed at Sapienza Università di Roma.

In this paper the SISAR model is applied to different stereo pairs (Castelgandolfo and Rome) and to point out the effectiveness of the new model, SISAR results are compared with the corresponding ones obtained by the software OrthoEngine 10.0 (PCI Geomatica).

By the University of Hannover a similar general satellite orientation program has been developed and the good results, achieved by bias corrected sensor oriented RPCs, for the test fields Mausanne (France) and Warsaw (Poland) have been described.

For some images, digital height models have been generated by automatic image matching with least squares method, analysed in relation to given reference height models. For the comparison with the reference DEMs the horizontal fit of the height models to each other has been checked by adjustment.

1. INTRODUCTION

Cartosat-1, also named IRS-P5, provides along track stereo imagery based on 2 cameras, having a view direction of 26° forward and 5° backward, leading to stereo models with just 53sec time difference in imaging. The camera configuration corresponds to a height to base relation (H/B) of 1.44 if the curvature of the orbit is respected. The 12000 pixels, each with 7x7 microns, in the image plane are covering with the focal length of 1.98m a swath of 30km with the forward view and 26.6km with the backward view. The GSD for a scene not rotated around the orbit direction is 2.5m x 2.78m respectively 2.22m x 2.23m. The incidence angle of 97.87° together with the flying height of 618km leads to a sun-synchronous orbit with 10:30 h equator crossing time in descending orbit. Cartosat-1 is equipped with a GPS receiver for the positioning and star sensors and gyros for the attitude determination. The satellite can be rolled around the orbit to image the requested area (Fig. 1).

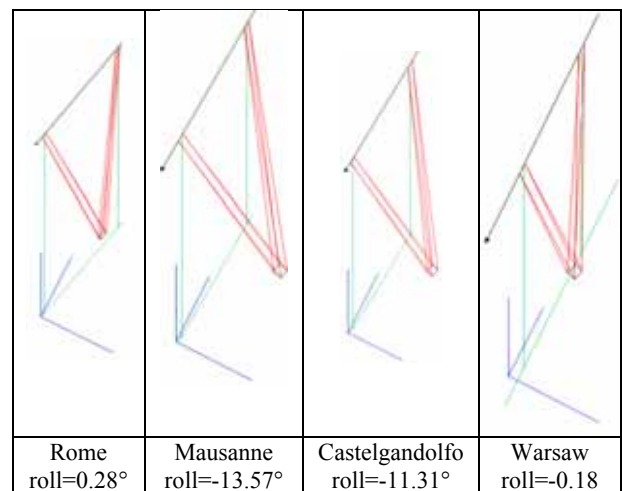


Fig. 1: imaging configuration of Cartosat-1

2. IMAGE ORIENTATION

The used satellite images have to be geo-referenced, this can be made by geometric reconstruction of the imaging, using orientation from the available metadata, improved by means of control points. The satellite information about the sensor orientation, based on GPS-positioning, gyros and star sensors is also distributed as rational polynomial coefficients (RPC). Approximate orientation procedures like 3D-affine transformation and DLT should not be used because of limited accuracy with basic images.

The application of 3D affine transformation (standard and adding 4 unknowns) and the DLT for the Castelgandolfo image gives accuracy much bigger than ground sampling distance (GSD) in across track direction both in aft and in fore camera, just when 10 unknowns in 3D affine are used the Root Mean Square Error (RMSE) are equal to 2*GSD (Fig. 2). In the satellite direction movement the worse accuracy is in aft image with a gap when minimum points necessary are used in DLT transformation (Fig. 3).

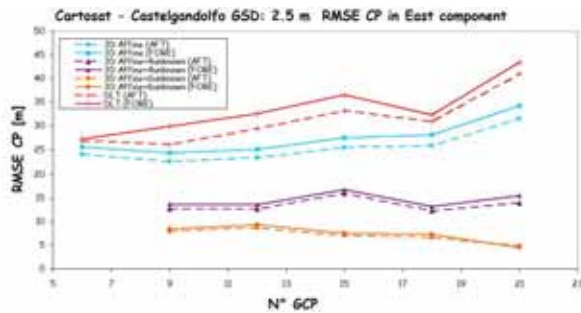


Fig. 2: RMSE at check points as function of the number of used control points of 3D Affine and DLT transformations [m] (East component)

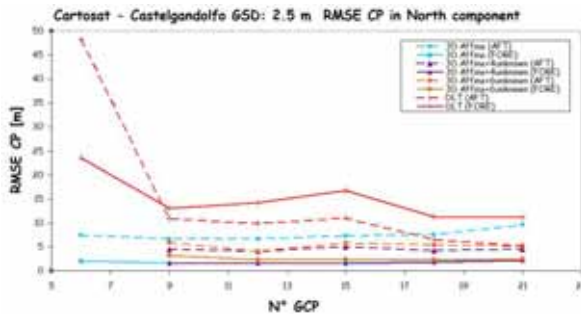


Fig. 3: RMSE at check points of 3D Affine and DLT transformations [m] (North component)

2.1 Sensor Oriented Rational Polynomial Coefficients

The replacement model of sensor oriented RPC describes the image coordinates I, J by the ratio of two 3rd order polynomials of the ground coordinates φ, λ, h (Jacobsen 2008). The direct sensor orientation without correction by control points is limited approximately to a standard deviation of 70m (Jacobsen et al 2008). This has to be improved by means of ground control points, named also as bias correction.

In an iterative procedure the geometric relation of the image to the 3D-ground coordinates is determined.

This needs a two-dimensional transformation to the control points. Experiences showed the requirement of a two-dimensional affine transformation, so for the 6 unknowns at least 3 control points are required (Tab. 1).

IMAGE		SINGLE		STEREO PAIRS		
		SX	SY	SX	SY	SZ
Mausanne	aft	2.4	2.1	2.1	2.7	3.4
	forward	2.0	2.1			
Warsaw	aft	1.4	1.5	1.3	1.1	1.8
	forward	1.4	1.3			

Tab. 1: RMSE at control points of bias corrected RPC orientation [m]

2.2 Geometric Reconstruction

Since 2003, the research group at the Area di Geodesia e Geomatica - Sapienza Università di Roma has been developing a specific model, based on geometric reconstruction, designed for the orientation of imagery acquired by pushbroom sensors carried on satellite platforms. This model has been implemented in the software SISAR (Software per Immagini Satellitari ad Alta Risoluzione). The RPC (use and generation) and orientation model of stereo pairs models are also implemented.

The model bases the imagery orientation on the well known collinearity equations including sets of parameters (Tab. 2) for the satellite position, the sensor attitude and the viewing geometry (internal orientation and self-calibration).

The sensor attitude is supposed to be represented by a known time-dependent term plus a 2nd order time-dependent polynomial, one for each attitude angle; moreover a rotation matrix in the Roll-Yaw plane is used for describe the canting for the two camera: the Fore and the Aft cameras are canted at +26° and -5° in the along track direction respectively (Crespi, 2008).

The atmospheric refraction is accounted by a general model for remote sensing applications (Noerdlinger, 1999). The viewing geometry is supposed to be modelled by the pixel size and two self-calibration parameters, able to account for a second order distortion along the array of detectors direction.

The approximate values of these parameters can be computed thanks to the information in the metadata file and these have to be corrected by a least square estimation process based on a suitable number of GCPs.

SATELLITE POSITION	Ω : right ascension of the ascending node i : orbit inclination e : satellite elevation at image centre α : satellite azimuth at image centre
SENSOR ATTITUDE	$\phi = \phi_0(t) + a_0 + a_1 t + a_2 t^2$ (roll) $\theta = \theta_0(t) + b_0 + b_1 t + b_2 t^2$ (pitch) $\psi = \psi_0(t) + c_0 + c_1 t + c_2 t^2$ (yaw)
VIEWING GEOMETRY	d_{pix} : pixel size I_0, J_0, d_1 : self-calibration parameters

Tab. 2: Full parametrization of the SISAR model

Not all parameters described in Tab. 2 are really estimable; actually, all the parameters related to the satellite position together with (I_0, J_0) are just computed according to the metadata information.

Moreover, as regards the remaining parameters, a methodology for the selection of the estimable ones is implemented in the software SISAR (Giannone, 2006). This methodology is able to avoid instability due to high correlations among some parameters leading to design matrix pseudo-singularity; it is based on Singular Value

Decomposition (SVD) and QR decomposition, employed to evaluate the actual rank of the design matrix, to select the estimable parameters and finally to solve the linearized collinearity equations system in the least squares (LS) sense. The SISAR model was tested on Cartosat-1 images with different features (for the features of all images see Tab. 3). All the images in forward looking (FORE) have a swath of 30km and in aft looking (AFT) have a swath 26.6km except Rome image that is not standard acquisition (swath 7.5km), since only a short part of the CCD array (3000 pixels vs. a total of 12000) was active.

Image	off-nadir angle (°)		Control points
	AFT	FORE	
Mausanne	14.45	29.10	32
Rome	4.97	26.09	43
Warsaw	4.97	26.04	29
Castelgandolfo	12.35	28.20	25

Tab. 3: Data set available

For the last images the showed results are focused on the DEM extraction rather than the orientation model.

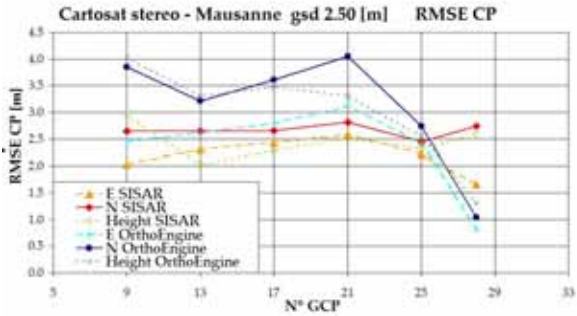


Fig. 4: RMSE at check points depending upon number of control points, trend for Mausanne image (North, East, Height components)

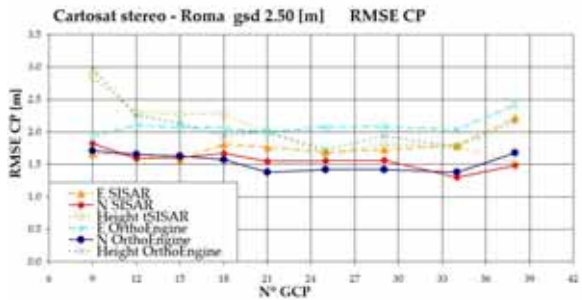


Fig. 5: RMSE at check points trend for Rome image (North, East, Height components)

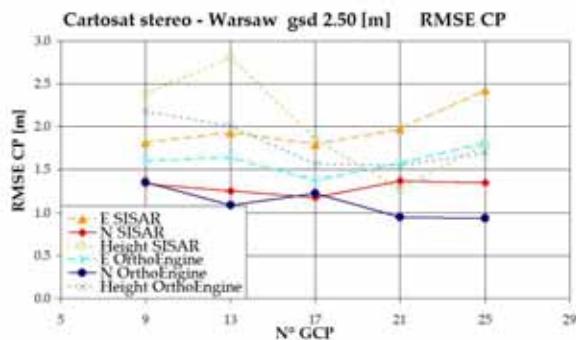


Fig. 6: RMSE at check points trend for Warsaw image (North, East, Height components)

The RMSE of check points (CPs) residuals, computed with SISAR software, underlines that the accuracies are similar to the GSD in horizontal and about H/B (1.60) multiplied for y-parallax (3.7m) in vertical. The similar results are obtained by OrthoEngine software with worse accuracy for Mausanne image and better accuracy for Warsaw image with respect to SISAR ones (Fig. 4,5,6).

2.2.1 RPC generation with geometric reconstruction

The RPCs can be generated according to a terrain-independent scenario, using known physical sensor model, or by terrain-dependent scenario without using any physical sensor models (Tao et al., 2001b). In the last method the solution is highly dependent on the actual terrain relief, the distribution and the number of GCPs and it does not provide a sufficiently accurate and robust solution if the above requirements for control information are not satisfied.

For the previous motivations, an innovative algorithm for the RPCs extraction, with a terrain independent approach, was implemented into the software SISAR. The basic steps of this algorithm are to build a 3D ground grid enveloping the terrain morphology of the imaged area starting from a rigorous orientation, and to estimate the RPCs that fit to this virtual space.

At first an image discretization was made, dividing the full extend image space in a 2D grid. Then the points of the 2D image grid are used to generate the 3D ground grid: the image was oriented and by the knowledge of the orientation sensor model the collinearity equations were derived and used to create the 3D grid, starting from each point of the 2D grid image. In this respect it has to be underlined that the 2D grid is actually a regular grid, whereas the 3D one is not strictly regular, due to the image attitude. Moreover, the 3D grid points were generated intersecting the straight lines modelled by the collinearity equations with surfaces (approximately ellipsoids) concentric to the WGS84 ellipsoid, placed at regular elevation steps.

So, the dimension of the 3D grid is both based on the full extent of the image and the elevation range of the terrain. The grid contains several elevation layers uniformly distributed, and the points on one layer have the same elevation value. The coarsest subdivision both for 2D grid definition and for layers spacing is dependent on the need to point out a sufficient points number for the RPCs estimation; on the other hand, the finest subdivision depends on the incompressible error of the geometric reconstruction used to generate the RPCs, so that a very fine discretization is useless and an upper discretization limit also exists.

The RPCs least squares estimation (Tao et Hu, 2000) is based on the linearization of the generic RPFs equations, which can be written as (1):

$$\begin{aligned}
 I_n + b_1 \lambda_n I_n + \dots + b_{17} \lambda_n^3 I_n + b_{18} h_n^3 I_n - a_0 - a_1 \varphi_n - \dots - a_{18} \lambda_n^3 - a_{19} h_n^3 &= 0 \\
 J_n + d_1 \lambda_n J_n + \dots + d_{17} \lambda_n^3 J_n + d_{18} h_n^3 J_n - c_0 - c_1 \varphi_n - \dots - c_{18} \lambda_n^3 - c_{19} h_n^3 &= 0
 \end{aligned}
 \quad (1)$$

where a_i , b_i , c_i , d_i are the RPCs (78 coefficients for third order polynomials), I_n , J_n and φ_n , λ_n , h_n are the normalized coordinates obtained through the equation (2) with scale and offset factors computed according to the equations (3):

$$T_n = \frac{T - T_{\text{offset}}}{T_{\text{scale}}} \quad \text{where } T = \varphi, \lambda, h, I, J \quad (2)$$

$$\begin{cases} w_{\text{offset}} = \min(w_k) \\ w_{\text{scale}} = \max(w_k) - \min(w_k) \\ I_{\text{offset}} = J_{\text{offset}} = 1 \\ I_{\text{scale}} = n^{\circ}\text{column} - 1 \\ J_{\text{scale}} = n^{\circ}\text{row} - 1 \end{cases} \quad \text{where } w = \varphi, \lambda, h \quad (3)$$

where k is the number of available ground control points (GCP) and n° column/row are the overall columns/rows of the image; the normalization range is (0, 1).

Deeper investigations underlined that many RPC coefficients are correlated; Tichonov regularization is usually used. On the contrary, in this work the Singular Value Decomposition (SVD) and QR decomposition are employed (Giannone, 2006).

For a system of linear equations ($Ax=b$), with $A \in \mathbb{R}^{m \times n}$ ($m \geq n$), a SVD-based subset selection procedure, due to Golub, Klema and Stewart (Golub et al., 1993; Strang et al., 1997), proceeds as follows:

- the SVD is computed and used both to calculate the approximate values of RPC to normalize the design matrix A and to determine the actual rank r of its; the threshold used to evaluate r is based on the allowed ratio between the minimum and maximum singular values; reference values are 10^{-4} – 10^{-5} (Press et al., 1992)
- an independent subset of r columns of A is selected by the QR decomposition with column pivoting $QR=AP$; in a system of linear equations ($Ax=b$), if A has a rank r , the QR decomposition produces the factorization $AP=QR$ where R is diagonal matrix, Q is orthogonal and P is a permutation (the permutation matrix P is calculated so that the columns of the matrix $B1 \in \mathbb{R}^{m \times r}$ in $AP=[B_1 B_2]$ are “sufficiently independent”)
- $B1$ is the matrix used to estimate the RPCs

Moreover, the statistical significance of each estimable coefficient is checked by a Student t -test so to avoid over-parametrization; in case of not statistically significant coefficient, it is removed and the estimation process is repeated until all coefficients are significant. In most of the cases the ‘degrees of freedom’ are high (more than 100), thus there could be considered infinite, converting the t -Student distribution in a normal standard distribution. The confidence interval chosen is 95%, so the value of the Student- t distribution was taken fixed to 1.96 (Millard, 2001).

Finally, the generated RPCs are used for the image orientation; in the SISAR software an algorithm is implemented for the RPCs application that allows also for a possible refinement process based on shift or affine transformation.

For each investigated image the RPCs (SISAR RPC) are been extracted using the known sensor model, implemented in SISAR software, with a specific number of GCPs and with a 3D grid (9x9x9), both sufficient conditions to have an accuracy assessment. The number of SISAR RPC are about 1/3 with respect to the standard number used in third order polynomial (78 RPC). The accuracy is, in worse case, close to 1.5 pixel when just 5 points are used (Tab. 4).

IMAGE	n° SISAR RPC		RMSE CP[pix]			
	AFT	FORE	AFT		FORE	
			I	J	I	J
Rome	22	24	0.93	0.61	1.26	1.04
Castelgandolfo	24	23	1.04	0.71	0.97	0.68
Warsaw	21	26	0.81	0.59	0.95	0.69
Mausanne	22	23	1.35	1.08	1.43	1.07

Tab. 4: SISAR RPC number and RMSE on CP for investigated images

3. IMAGE MATCHING

The image orientation is only the precondition for the geometric correct use of the image information. One important issue of the stereo satellite Cartosat-1 is the generation of height models. With the spectral range from 0.50 up to 0.85 μ m wavelength large parts of the near infrared are included, giving optimal conditions also over forest areas.

An automatic image matching has been made with the Hannover program DPCOR. It is imbedded in the measurement program DPLX allowing a fast check of the matched points. DPLX is using a least squares matching, having no accuracy limitations for inclined areas like the image correlation. The least squares image matching includes an affine transformation of the sub-matrix of one image to the sub-matrix of the other image. In addition a constant shift and linear changes of the grey values with both coordinates are included, leading to 9 unknowns. The precise matching by least squares has a disadvantage of a low convergence radius – the corresponding image positions must be known on a higher level. In DPCOR this is solved by region growing. Starting from at least one corresponding point, the neighbored points are matched. Such a seed point may be a control point, which has to be measured in any case manually. By matching the neighbored points the geometric relations are improved before going to the next neighbored points. DPCOR is always following the path with the highest correlation coefficient up to the complete coverage of the stereo pair with corresponding points having a correlation coefficient above a chosen threshold. The threshold for Cartosat-1 images may be the correlation value of 0.6. Usually only a limited number of useful points is located below this limit. Of course if the area has no variation of the grey values, a matching is not possible (Fig. 7).

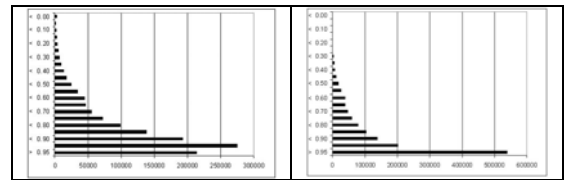


Fig. 7: frequency distribution of correlation coefficient horizontal: frequency vertical: correlation coefficient - above $r=0.0$ below $r=1.0$ (Mausanne-left, Warsaw-right)

Fig. 7 shows the frequency distribution of the correlation coefficients. In the Mausanne model the object contrast was limited because of the winter, so that the highest number of correlation coefficients is in the group $r=0.90$ up to 0.95, Warsaw in the class $r=0.95$ up to 1.0. In relation to other satellites, the matching with Cartosat-1 models is extremely successful. The overlay of the matched and accepted points to one of the scenes in figure 8 demonstrates the successful solution. In the Mausanne scene in some parts absolute no contrast was on the ground. In Warsaw slight snow coverage caused some problems (Fig.8).

Regarding the stereo pair of Castelgandolfo the matching was really good (Fig. 9) and the not matched points are mainly due to the lakes and to the clouds, which cover together a big part of the images. In Fig. 9 the matched points distribution over the after image is shown on the left, and on the right the trend of the correlation coefficient (r) is

represented using grey values 0 for the $r=0$ and grey values 255 for $r=1$.

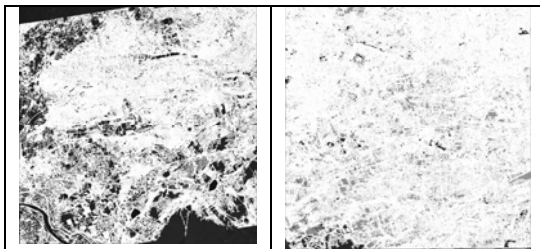


Fig. 8: overlay of matched points (white) to after scenes (Mausanne-left, Warsaw-right)

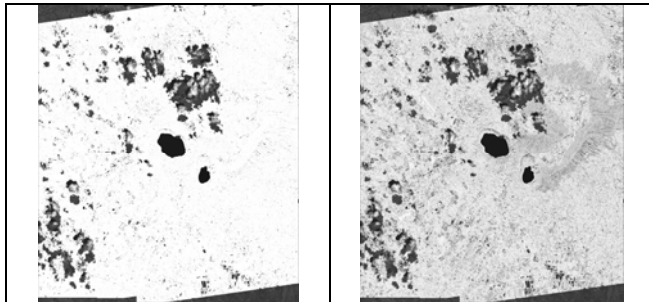


Fig. 9: matched image points (left) and quality image (grey values correspond to correlation coefficient) of Castelgandolfo

In Fig. 10 frequency distribution of the correlation coefficients for the Castelgandolfo stereo pair is shown. The highest number of correlation coefficients is in the group $r=0.90$ up to 0.95 ; this distribution is due to the soil coverage (forest and lakes) and to the clouds on the image.

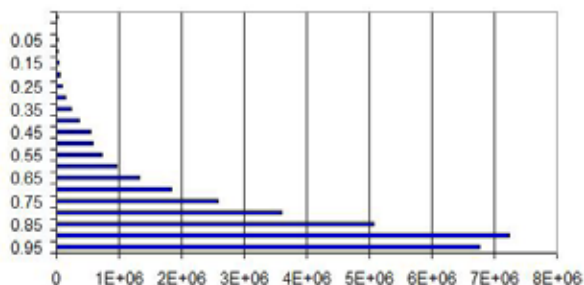


Fig. 10: frequency distribution of correlation coefficient (Castelgandolfo)

For the Castelgandolfo stereo pair, based on the scene orientation obtained with the RPC generated from SISAR, and after the automatic image matching, the digital surface model has been generated using the Hannover software RPCDEM, and compared with a precise reference DSM extracted by aerial photos.

On the contrary Mausanne and Warsaw DSM have been extracted using the RPC supplied with the image.

In the open areas of Mausanne, the height model was even more precise than the accuracy estimated by means of the RMSE y-parallax (2.87m). Of course the generated DSM showing the height of the visible surface has to be filtered for objects not belonging to the bare ground because the reference DEM is related to this (Tab. 5).

For Castelgandolfo's scene the RMSE y-parallax of 4 million points was 1.79m, corresponding to a standard deviation of the height of 2.86m.

Image	Area	SZ	bias	SZ = $f(\alpha=\text{inclination})$
Mausanne	no filter	4.02*	-0.51	$3.91 + 1.64 \cdot \tan \alpha$
	yes filter	3.30*	0.48	$3.17 + 3.14 \cdot \tan \alpha$
Warsaw	no filter	3.23*	-0.54	$3.16 + 1.19 \cdot \tan \alpha$
	yes filter	2.43*	0.44	$2.39 + 8.80 \cdot \tan \alpha$
Castelgandolfo	no filter	2.88*	-0.06	$2.71 + 0.41 \cdot \tan \alpha$
	yes filter	2.29*	0.30	$2.26 + 0.17 \cdot \tan \alpha$
	no filter	4.67**	-0.58	$3.95 + 1.64 \cdot \tan \alpha$
	yes filter	4.06**	-0.34	$3.27 + 1.91 \cdot \tan \alpha$

Tab. 5: accuracy of Cartosat-1 height models checked by precise reference DEMs[m] (*referred to open area, **referred to urban area) (Jacobsen 2006)

The reference aerial DSM covers an area of about 85km^2 in the centre of the scene, including forest parts and both open and urban areas. These result are satisfying considering that the area of interest is full of elements that do not belong to the bare ground (like trees or buildings).

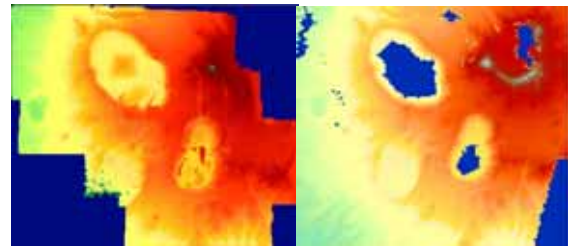


Fig. 11: colour coded height model extracted from aerial images (left) and from Cartosat-1 images (right)

In Fig.11 the extracted height models are shown; the software used for the DEM generation are respectively ERDAS v. 9.1 for the aerial block and RPCDEM for Cartosat-1 stereo pairs. The two software packages respond in different ways in the lake zone, in fact ERDAS applies an automatic filtering function so that it is able to assign an elevation even in the lake areas, on the contrary the matching achieved by DPLX did not recognize homologous points for the two images, due to the fact that no contrast was available on the lakes; therefore the elevation of those points was not extracted by RPCDEM.

Furthermore the accuracy of Cartosat-1 DSM has been checked, with respect to the reference DSM over different terrain types: open areas and urban areas; thus the overall scene has been divided in several selected regions. The analyses have been performed both for the digital surface models directly obtained from the images, and for the digital elevation models, obtained filtering the original DSMs with the Hannover software RASCOR.

The selected open regions are not completely flat zones, because they still contain sparse buildings and groups of trees, nonetheless the accuracy obtained was in the range of the standard deviation of the height.

Regarding the urban areas the discrepancies with the reference DSM are bigger; in these areas the smoothing effect of Cartosat-1 is more evident, in fact, while the DSM results higher than the reference over the streets, it tends to smooth the edges of the buildings, as it is shown by the profiles in Fig 12; on the contrary after filtering the profiles are similar and the smoothing effects disappear (Fig. 13).

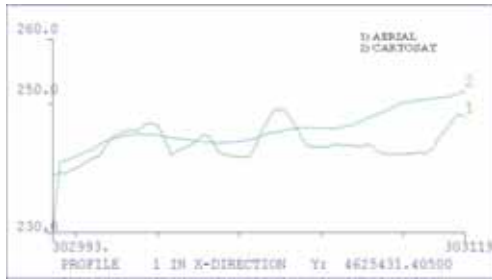


Fig. 12: profiles through a Cartosat-1 DSM and the reference DSM from aerial images an urban area

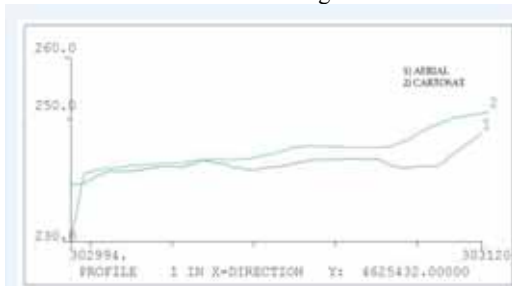


Fig. 13: profiles through a Cartosat-1 DEM and the reference DEM from aerial images an urban area

In the Fig. 14 the differential DSM of an open area and an urban area are shown; the differential DSM is obtained by the comparison between the DSM reference and the Cartosat-1 DSM generated with RPCDEM using the SISAR RPC (Fig. 14).

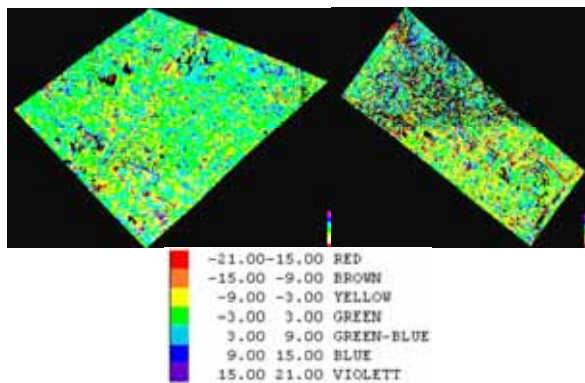


Fig. 14: Differential DSM of open area (left) and urban area (right)

7. CONCLUSION

Results stemming from the geometric reconstruction of Cartosat-1 imagery shows that accuracy is at GSD level in horizontal components and at about 2-3 m in vertical one.

The SISAR results demonstrate that RPCs, generated by SISAR software, permit high performance for image orientation, achieving results close to the geometric reconstruction. A particular core was devoted into the estimable coefficient selection; by now the usual strategy is the mainly based on Tichonov regularization, on the contrary, in this work a different innovative method was used, based on the Singular Value Decomposition (SVD) and QR that can reliably handle the rank deficient matrices, without require an empirical evaluation of the regularization parameter. This selection allows to use a number of coefficients lower than the standard number used in the third order polynomial (78 RPC).

Digital height models have been generated by means of Cartosat-1 stereo pairs. The orientation of the models in any case was possible with sub-pixel accuracy by bias corrected RPC-solution. In any case for flat terrain the height accuracy is better than 1 GSD for the x-parallax or 4m. After filtering for elements not belonging to the bare ground the vertical accuracy for flat terrain is not less than 3.2m corresponding to x-parallax accuracy of 0.8 GSD. In relation to other optical space sensors this is a very good result.

For the stereo scenes of Castelgandolfo the DSM was generated using the orientation achieved with the RPC extracted by SISAR. Cartosat-1 DSM was compared with a precise reference from aerial images and the results achieved show the goodness of the model. From DSM comparison in the open areas an SZ of 2.88m is achieved, while in the urban areas the SZ is around 4.67m. The latter value, in urban area, is due to the lower resolution of satellite imagery with respect to the aerial images, which causes a smoothing effect in the Cartosat-1 DSM.

The GSD of 2.5m also allows the generation of the main structures of build up areas.

REFERENCES

- Crespi, M., Fratarcangeli, F., Giannone, F., Jacobsen K., F. Perialice 2008: Orientation of Cartosat-1 Stereo Imagery, EARSeI, Workshop Remote Sensing - New Challenges of High Resolution, Bochum 2008
- Giannone, F., 2006. A rigorous model for High Resolution Satellite Imagery Orientation. Phd Thesis Sapienza Università di Roma (<http://w3.uniroma1.it/geodegeom/personale.htm>)
- Golub, G. and Van Loan, C. F., 1993. Matrix computation. The Johns Hopkins University Press, Baltimore and London.
- Jacobsen K., 2006: ISPRS-ISRO Cartosat-1 Scientific Assessment Jptogramme (C-SAP) Technical report - test areas Mausanne and Warsaw, ISPRS Com IV, Goa 2006, IAPRS Vol. 36 Part 4, pp. 1052-1056
- Jacobsen, K., Crespi, M., Fratarcangeli, F., Giannone, F., 2008.: DEM generation with Cartosat-1 stereo imagery EARSeI, Workshop Remote Sensing - New Challenges of High Resolution, Bochum 2008
- Jacobsen, K., 2008: Satellite image orientation, ISPRS congress Beijing (WG I/5)
- Millard, S.P., Neerchal, N.K.; 2001. Environmental Statistic. CRC Press.
- Noerdlinger, P. D., 1999. Atmospheric refraction effects in earth remote sensing. ISPRS Journal of Photogrammetry & Remote Sensing 54, pp. 360-373.
- Press, W. H., Teukolski, S. A., Vettering, W. T., Flannery, B. P., 1992. Numerical Recipes in Fortran. Cambridge University Press, Cambridge.
- Tao, C.V., Hu, Y., 2000. Investigation of the Rational Function Model. Proceedings of ASPRS Annual Convention, Washington D.C.
- Tao, C.V., Hu, Y., 2001b. A comprehensive study of the rational function model for photogrammetric processing. Photogrammetric Engineering & Remote Sensing. 67(12), pp. 1347-1357.